JOURNAL OF COMPUTATIONAL PHYSICS 112, 253–266 (1994)

A Truly Noninterpolating Semi-Lagrangian Lax–Wendroff Method

M. OLIM*

Institute of Fluid Science, Tohoku University, Sendai, Japan

Received October 16, 1992

A truly noninterpolating semi-Lagrangian method has been developed. It is based upon a modification of a standard Lax–Wendroff scheme and is unconditionally stable on a regular rectangular grid. The method is explicit and second-order accurate in both time and space. It is suggested that the computational cost and memory allocation required by this method are the least possible for a semi-Lagrangian algorithm of this order of accuracy. The numerical experiments presented indicate that the algorithm is very accurate indeed.

1. INTRODUCTION

The evolution of a large number of physical systems may be described, either entirely or in part, by the following partial differential equation:

$$\frac{\partial \phi}{\partial t} + \mathbf{u} \cdot \nabla \phi = \nu \nabla^2 \phi + f, \tag{1}$$

where $\mathbf{u}$ is the velocity vector and the functions ϕ, ν, and f may have a variety of physical interpretations. In the context of fluid dynamics (1) may describe, for example, the advection–diffusion of a temperature field in which case ϕ, ν, and f represent, respectively, nondimensional temperature, space-independent thermal conductivity, and heat generation rate. The advection–diffusion of a velocity component in a solenoidal fluid flow with negligible second viscosity may also be described by (1) in which case ϕ, ν, and f represent, respectively, nondimensional velocity component, kinematic viscosity, and a combination of internal and external forces.

We are specifically interested in an often-encountered class of advection–diffusion equations in which the typical magnitude of the advective velocity, $\mathbf{u}$, is sufficiently high so that the second term on the left-hand side of (1) dominates either of the terms on the right-hand side. Such equations are referred to as advection dominated. This paper focuses on the numerical simulation of the advection process.

2. SEMI-LAGRANGIAN SCHEMES

Explicit Eulerian schemes employed to approximate the advection process are often subject to a constraint which imposes an upper limit on the Courant number such as, for example, the CFL stability condition (this subject is thoroughly covered in intermediate level treatments such as, for example, [9, 12]). Implicit Eulerian schemes, although often unconditionally stable, exhibit damping which increases rapidly with the Courant number. Consequently, the magnitude of the time step in Eulerian schemes is usually restricted, due to considerations of either stability or damping, by a value which may be significantly smaller than a typical time interval related to the temporal scale on which the system of interest actually evolves. In advection-dominated equations the hyperbolic character of the transport process may be exploited, which leads to the use of Lagrangian schemes. From the numerical stability perspective the conceptual difference between Eulerian and Lagrangian schemes is simply that the stability of an Eulerian scheme is related to the *magnitude* of the advective velocity while the stability of a Lagrangian scheme is related to the *variation* of the advective velocity. For example, if the velocity is constant then there is no numerical reason to restrict the time step of a Lagrangian scheme. This difference between Eulerian and Lagrangian schemes is expressed by the fact that the former are usually more restrictive than the latter in so far as the time step is concerned. The drawback of Lagrangian schemes lies in the fact that following fluid particles may lead to deterioration of the spatial resolution in some parts of the domain. It seems therefore that the best of both worlds may be achieved by the use of semi-Lagrangian schemes.

In a semi-Lagrangian scheme the grid points are stationary and the fluid particles are advected using a Lagrangian scheme for a single time step. The information is then projected onto the stationary grid. A different set of fluid particles is chosen for advection at each time step, and they are chosen so as to arrive at the precise locations of the

* Permanent address: FSI International, 322 Lake Hazeltine Dr., Chaska, Minnesota 55318-1096.

0021-9991/94 $6.00

grid points. Thus, the resolution of the domain remains regular, and the magnitude of the time step is not restricted by the constraints of Eulerian schemes. To outline the essentials of a general semi-Lagrangian scheme let us assume that the right-hand side of (1) may be represented by some function $R_{(\phi,\mathbf{x},t)}$. We are therefore concerned with constructing a numerical solution to the differential equation,

$$\frac{d\phi}{dt}=\left(\frac{\partial}{\partial t}+\mathbf{u}\cdot\nabla\right)\phi=R \tag{2}$$

which describes the change of ϕ along a characteristic

$$\frac{d\mathbf{x}}{dt}=\mathbf{u}. \tag{3}$$

If the material derivative is approximated by an $O(\Delta t^2)$ accurate three-time-level explicit scheme then the numerical equivalent of (2) is

$$\phi_{(\mathbf{x}_i,t^{n+1})}=\phi_{(\mathbf{x}_i-2\Delta t\,\mathbf{u},t^{n-1})}+2\Delta t\,R_{(\mathbf{x}_i-\Delta t\,\mathbf{u},t^n)}, \tag{4}$$

where $\mathbf{x}_i$ represents the coordinates of grid point $\mathbf{i}$ in the (multidimensional) domain and $\mathbf{x}_i-2\Delta t\,\mathbf{u}$ is the departure point of the fluid particle arriving at $\mathbf{x}_i$.

In general, neither the departure point of a fluid particle, $\mathbf{x}_i-2\Delta t\,\mathbf{u}$, nor the point the which R must be evaluated, $\mathbf{x}_i-\Delta t\,\mathbf{u}$, coincide with a grid point. Therefore the terms on the right-hand side of (4) must be determined by interpolation of data known at the time levels t^n and t^{n-1}. Robert [10] suggested that this explicit three-time-level method may be replaced by a semi-implicit two-time-level method of the same, $O(\Delta t^2)$, accuracy by halving the advection time interval used in (4), yielding the equation,

$$\phi_{(\mathbf{x}_i,t^{n+1})}=\phi_{(\mathbf{x}_i-\Delta t\,\mathbf{u},t^n)}+\tfrac{1}{2}\Delta t\,[R_{(\mathbf{x}_i,t^{n+1})}+R_{(\mathbf{x}_i-\Delta t\,\mathbf{u},t^n)}], \tag{5}$$

where $\mathbf{x}_i-\Delta t\,\mathbf{u}$ is the departure point of the fluid particle. This scheme requires interpolation of data at the time level t^n and evaluation of R as an average between the fluid particle points of departure and arrival in the time-space domain. The schemes suggested by (4) and (5) establish the basis of the traditional forms for semi-Lagrangian methods (see [14] for a recent review and list of references). Another typical semi-Lagrangian scheme, although not referred to as such, is described in [5]. In this scheme, which is only first-order accurate in time, the departure point of the particle is a grid point and at the end of the time step the advected property is distributed among the grid points surrounding the arrival point. All schemes mentioned so far require spatial interpolation of data either at the beginning or at the end of the advection time interval. Such interpolation may lead to smoothing and constitutes an extremely costly operation.

An alternative method which requires no interpolation at any of these time levels was suggested in [11]. This method is based on the following modification of (2),

$$\frac{\partial\phi}{\partial t}+\mathbf{u}\cdot\nabla\phi=\frac{\partial\phi}{\partial t}+(\mathbf{u}_I+\mathbf{u}_R)\cdot\nabla\phi=R, \tag{6}$$

rewritten as

$$\frac{\partial\phi}{\partial t}+\mathbf{u}_I\cdot\nabla\phi=R-\mathbf{u}_R\cdot\nabla\phi \tag{7}$$

which describes the change of ϕ along a characteristic

$$\frac{d\mathbf{x}}{dt}=\mathbf{u}_I \tag{8}$$

and where $\mathbf{u}_R=\mathbf{u}-\mathbf{u}_I$ is the velocity vector connecting the fluid particle departure point to the nearest grid point. The remainder of the velocity, $\mathbf{u}_I$, is the velocity vector connecting that grid point to the (grid) point at which the fluid particle will arrive. On a grid in which the grid points are located along lines parallel to the spatial axes $\mathbf{u}_I=\mathbf{p}\cdot\Delta\mathbf{x}/\Delta t$, where the components of the vector $\mathbf{p}$ represent the (integer) number of grid lengths traveled by a fluid particle in each spatial direction during the advection time interval. The ith component of the vector $\mathbf{p}$ is evaluated using the ith component of the velocity vector $\mathbf{u}$ and the grid length in the ith direction,

$$p_i=\mathrm{nint}(C_i), \tag{9}$$

where $\mathrm{nint}(C_i)$ indicates the integer nearest C_i, and $C_i=u_i\,\Delta t/\Delta x_i$ is the Courant number in the ith direction. In other words, the ith component of $\mathbf{u}_I$ is chosen in such a manner that the fluid particle arriving at a grid point departs p_i grid points away. It should be noted that if $C_i<0.5$ then $p_i=0$, in which case a noninterpolating semi-Lagrangian scheme is equivalent to an Eulerian scheme. An $O(\Delta t^2)$ accurate approximation of (7) is the three-time-level scheme,

$$\phi_{(\mathbf{x}_i,t^{n+1})}-\phi_{(\mathbf{x}_i-2\Delta t\,\mathbf{u}_I,t^{n-1})}=2\Delta t\,(R-\mathbf{u}_R\cdot\nabla\phi)_{(\mathbf{x}_i-\Delta t\,\mathbf{u}_I,t^n)}, \tag{10}$$

where $(\mathbf{x}_i-2\Delta t\,\mathbf{u}_I)$ is the grid point nearest the departure point of the fluid particle. This is the original method suggested by Ritchie in [11] and it was termed noninterpolating. Although this method eliminates the interpolation related to the data at the departure point of the fluid particle, the point at which the right-hand side of (10) is

evaluated, $(\mathbf{x}_i - \Delta t\, \mathbf{u}_I)$, does not in general coincide with a grid point. Therefore the formulation (10) still requires interpolation of data at the time level t^n. This is true even for pure advection, i.e., $R = 0$.

To complete this very brief review of semi-Lagrangian methods, there exists yet an additional method that is useful (mostly) for conversion of an Eulerian scheme to a semi-Lagrangian scheme. This method suggests the employment of an Eulerian scheme for advection from the particle departure point to the nearest grid point and then a Lagrangian scheme for advection from there to the arrival grid point [13].

3. A NONINTERPOLATING SEMI-LAGRANGIAN LAX–WENDROFF METHOD

Lax–Wendroff methods are traditionally employed for the solution of the following forcing- and dissipation-free equation:

$$\frac{\partial \phi}{\partial t} = -\mathbf{u} \cdot \nabla \phi. \tag{11}$$

The noninterpolating (semi-) Lagrangian advection formulation, on the other hand, requires the solution of the equation,

$$\frac{d\phi}{dt} = -\mathbf{u}_R \cdot \nabla \phi. \tag{12}$$

The similarity between these two equations is obvious. The dependent variable ϕ may be expanded *along a characteristic* using the single-variable Taylor series,

$$\phi_{t+\Delta t} = \phi_{(t)} + \sum_{m=1}^{\infty} \frac{\Delta t^m}{m!} \frac{d^m \phi}{dt^m}, \tag{13}$$

and the one-step noninterpolating semi-Lagrangian Lax–Wendroff method consists of the substitution of

$$\frac{d^m}{dt^m} = (-\mathbf{u}_R \cdot \nabla)^m, \qquad m = 1, 2, ..., \tag{14}$$

into (13). After this substitution the semi-Lagrangian two-time-level explicit scheme of $O(\Delta t)^2$ accuracy may be obtained,

$$\phi_{(\mathbf{x}_i, t^{n+1})} = \phi_{(\mathbf{x}_i - \Delta t\, \mathbf{u}_I, t^n)} + \left[\sum_{m=1}^{2} \frac{\Delta t^m}{m!} (-\mathbf{u}_R \cdot \nabla)^m \phi \right]_{(\mathbf{x}_i - \Delta t\, \mathbf{u}_I, t^n)}, \tag{15}$$

where $(\mathbf{x}_i - \Delta t\, \mathbf{u}_I)$ represents the coordinates of the fluid particle departure (grid) point. If $\mathbf{u}_R = \mathbf{u}$ then $\mathbf{u}_I = 0$, the material derivative in (14) is replaced by a partial derivative with respect to time, and the semi-Lagrangian formulation (15) reduces to a traditional (i.e., Eulerian) Lax–Wendroff scheme.

The temporal accuracy of (15) may be improved by including higher order terms in the summation on the right-hand side of (15) and/or by averaging the summation between the grid points of particle departure and arrival in the time-space domain. An alternative method of achieving this goal for an Eulerian advection scheme was presented by Donea in [3]. This method is based upon a semi-discrete representation of (11) and is known in the "finite element world" as the Taylor–Galerkin method. In this scheme the Lax–Wendroff method is employed to calculate the $O(\Delta t)$ and the $O(\Delta t)^2$ terms, but rather than evaluating the $O(\Delta t)^3$ term in (13) using a higher spatial derivative, as prescribed by (14), the term is evaluated using the approximation,

$$\frac{\partial^3 \phi}{\partial t^3} = \frac{\partial}{\partial t} (\mathbf{u} \cdot \nabla)^2 \phi = (\mathbf{u} \cdot \nabla)^2 \frac{\partial \phi}{\partial t} \approx (\mathbf{u} \cdot \nabla)^2 \frac{\phi_{(\mathbf{x}_i, t^{n+1})} - \phi_{(\mathbf{x}_i, t^n)}}{\Delta t}, \tag{16}$$

where use is made of

$$\frac{\partial^2}{\partial t^2} = (\mathbf{u} \cdot \nabla)^2, \tag{17}$$

and the remaining first-order partial time derivative is approximated by forward Euler differencing. The Taylor–Galerkin method may employ any time-differencing scheme, and the forward Euler method is chosen here only to illustrate the basic principles. The resulting version of (11) is the equation

$$[1 - \tfrac{1}{6}(\Delta t\, \mathbf{u} \cdot \nabla)^2]\, \phi_{(\mathbf{x}_i, t^{n+1})} = [1 - \Delta t\, \mathbf{u} \cdot \nabla + \tfrac{1}{3}(\Delta t\, \mathbf{u} \cdot \nabla)^2]\, \phi_{(\mathbf{x}_i, t^n)} \tag{18}$$

which is discrete in time but continuous in space and hence termed semi-discrete. Although originally suggested as a finite element method this semi-discrete equation may also be used in a finite difference formulation. The method may be converted to a semi-Lagrangian form by substituting $\mathbf{u}_R$ and $\phi_{(\mathbf{x}_i - \Delta t\, \mathbf{u}_I, t^n)}$ for $\mathbf{u}$ and $\phi_{(\mathbf{x}_i, t^n)}$ in (18).

Another interesting finite element method which makes use of *advected* weighting functions was suggested by Benque *et al.* in [1]. The basic principle of this method may be illustrated by applying it to the following conservation equation.

$$\frac{\partial \phi}{\partial t} + \mathbf{u} \cdot \nabla \phi = 0. \tag{19}$$

To obtain the weak formulation (19) is multiplied by a weighting function ψ_j and integrated over the spatial

domain Ω and, contrary to the usual practice, also over the time step Δt, thus yielding the equation

$$\int_{\Omega} [(\phi\psi_j)^{n+1} - (\phi\psi_j)^n] - \int_{\Omega}\int_{\Delta} \phi\left(\frac{\partial\psi_j}{\partial t} + \mathbf{u}\cdot\nabla\psi_j\right) = 0, \quad (20)$$

where, for simplicity, a solenoidal velocity vector and homogeneous boundary conditions were assumed. The time dependent weighting functions are conserved along the characteristics; therefore the second integral in (20) vanishes. To provide a distribution for the weighting functions at some point of time, they are made to coincide with the basis functions at the end of a time step, viz.,

$$\psi_j(\mathbf{x}, t^{n+1}) = \xi(\mathbf{x}) \quad (21)$$

where $\{\xi\}$ are the basis functions used to approximate the dependent variable ϕ.

Karpik [7] developed Benque's scheme further and conducted a series of numerical experiments showing that the results provided by this scheme are superior to those provided by Ritchie's scheme and by two widely used finite element methods, namely the streamline upwind/Petrov–Galerkin [6] and the Taylor–Galerkin methods. However, to different extents, they all suffer from undershoots (as shown in [7]) and will therfore generate unacceptable results when simulating advection of a property which is positive definite such as, for example, density of a compressible fluid or moisture in the atmosphere. While all three finite element schemes exhibit performance which is superior to that of a finite difference Lax–Wendroff scheme, the performance of a Lax–Wendroff scheme may be considerably improved at relatively low cost by the use of a monotonicity preserving method such as the flux corrected transport (FCT), the total variation diminishing (TVD), or the essentially non-oscillating (ENO) methods; a detailed treatment of the FCT and the TVD methods and an extensive list of references are provided in [8], and the ENO method is described in [4].

One is then faced with the issue of the relative efficiency of the Lax–Wendroff and Benque methods described above. Like all finite element methods Benque's scheme is implicit, thus resulting in a system of equations which must be solved simultaneously. Unless the problem is one-dimensional and linear basis functions are used, in which case a tri-diagonal matrix is obtained and the Thomas algorithm [9] may be employed, the solution of such systems requires a number of floating point operations which is proportional to N^s, where N is the number of degrees of freedom of the system and s is always greater than one. On the other hand, implementation of the FCT method with the explicit Lax–Wendroff scheme requires a number of floating point operations which is proportional to N. Clearly, the FCT-modified Lax–Wendroff method will be more efficient than Benque's scheme and any other finite element method.

Since the stability restriction of the explicit Eulerian formulation is circumvented by semi-Lagrangian schemes it seems that implicit schemes (both Eulerian and semi-Lagrangian) offer no compensation for the additional cost of their implementation. Further discussion will therefore be focused upon the explicit finite difference semi-Lagrangian Lax–Wendroff scheme. A monotonicity preserving method such as the FCT may be implemented with the explicit semi-Lagrangian Lax–Wendroff scheme given by (15). Compared to Eulerian Lax–Wendroff schemes the semi-Lagrangian version requires no additional steps in order to implement the FCT method. The one-dimensional version of (15) was implemented using centered differences to compute the spatial derivatives and modified using the FCT method (see Phoenical Lax–Wendroff in [2]). An initial test was performed in which a square wave 20 grid lengths wide was advected using a Courant number of 2.5. For reasons which will be explained later a Courant number whose noninteger part is 0.5 provides the most stringent test of the semi-Lagrangian Lax–Wendroff algorithm. Using periodic boundary conditions the square wave was advected five times through a domain represented by 100 grid points, and the analytical and numerical solutions are shown in Fig. 1. The five crossings of the domain required 200 time steps, and the results shown in the figure indicate that the algorithm performs extremely well.

4. ANALYSIS OF THE SUGGESTED SCHEME IN TWO DIMENSIONS

A quadrilateral grid, the computational molecule for which is shown in Fig. 2a, may be easily mapped onto a regular rectangular grid. For this purpose new axes, x' and y', may be defined in a manner such that the grid points are located along them as shown in the figure. The resulting computational molecule is shown in Fig. 2b. The noninterpolating semi-Lagrangina Lax–Wendroff scheme will therefore be analyzed on the regular rectangular grid. On this grid a grid point belongs to and is surrounded by four rectangles. Let the grid points belonging to this computational molecule be numbered as shown in Fig. 2b, and let the dimensions of each rectangle be $\Delta x \times \Delta y$.

4.1. *The Lax–Wendroff Method Using the Taylor Expansion in Space*

The spatial derivatives at the center point of the computational molecule may be evaluated using a finite difference formulation. For this purpose the values of the dependent variable ϕ at the eight outer points of the computational

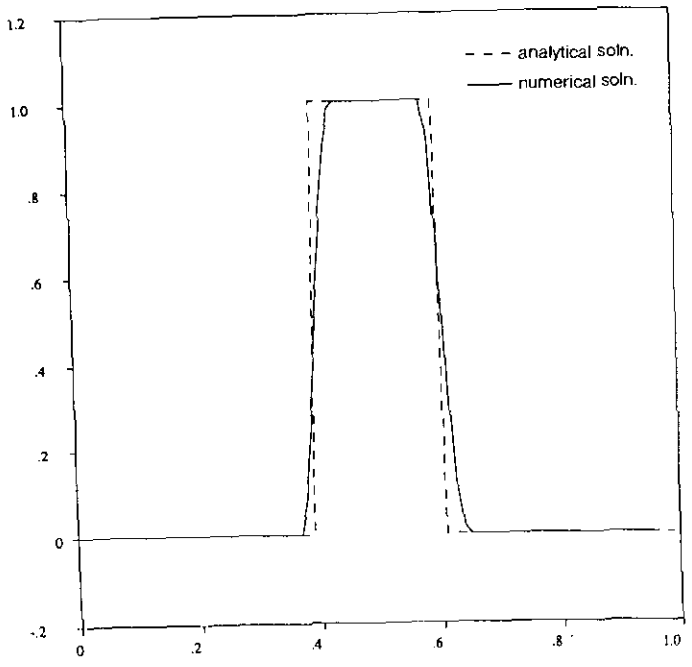

FIG. 1. Numerical and analytical results of a one-dimensional advection of a square wave. The wave was advected through the domain five times. The numerical results (solid line) were obtained for a Courant number of 2.5 using the noninterpolating semi-Lagrangian Lax–Wendroff method with FCT.

molecule shown in Fig. 2b are approximated using the multidimensional Taylor series, viz.,

$$\phi_k \approx \phi_0 + \phi_x \Delta x_k + \phi_y \Delta y_k + \tfrac{1}{2}\phi_{xx} \Delta x_k^2 + \phi_{xy} \Delta x_k \Delta y_k + \tfrac{1}{2}\phi_{yy} \Delta y_k^2, \tag{22}$$

where the subscript k indicates the number of the outer point (1 to 8), the subscripts x and y indicate partial derivatives, and Δx_k, Δy_k are the distances from point k to point 0. Using (22) the spatial derivatives ϕ_x, ϕ_y, ϕ_{xx}, ϕ_{xy}, and ϕ_{yy} required in (15) may be calculated by appropriately choosing five out of the eight points surrounding the center point. For best results, we use the points numbered 2, 4, 6, and 8, and one of the corner points numbered 1, 3, 5, or 7. These four combinations yield the same formulae for ϕ_x, ϕ_y, ϕ_{xx}, and ϕ_{yy}, and, for improved accuracy, the formula used for ϕ_{xy} is the average of the formulae obtained from the four combinations, viz.,

$$\phi_x = \frac{\phi_{i+1,j} - \phi_{i-1,j}}{2\Delta x}, \qquad \phi_{xx} = \frac{\phi_{i+1,j} - 2\phi_{i,j} + \phi_{i-1,j}}{\Delta x^2},$$
$$\phi_y = \frac{\phi_{i,j+1} - \phi_{i,j-1}}{2\Delta y}, \qquad \phi_{yy} = \frac{\phi_{i,j+1} - 2\phi_{i,j} + \phi_{i,j-1}}{\Delta y^2}, \tag{23}$$
$$\phi_{xy} = \frac{\phi_{i-1,j-1} + \phi_{i+1,j+1} - \phi_{i+1,j-1} - \phi_{i-1,j+1}}{4\Delta x\, \Delta y},$$

where i and j are grid point indices in the x and y directions, respectively.

During the time step a fluid particle is advected from the grid point (x_i, y_j) to the grid point (x_{i+p}, y_{j+q}), viz.,

$$\Delta t\, \mathbf{u}_I = p\, \Delta x\, \hat{\mathbf{i}} + q\, \Delta y\, \hat{\mathbf{j}}. \tag{24}$$

Introduction of (23) and (24) into (15) yields the equation

$$\phi_{i+p,j+q}^{n+1} = \phi_{i,j}^n (1 - C_x^2 - C_y^2) + \frac{C_x C_y}{4} \times (\phi_{i-1,j-1}^n + \phi_{i+1,j+1}^n - \phi_{i+1,j-1}^n - \phi_{i-1,j+1}^n) + \frac{C_x}{2}[\phi_{i-1,j}^n (1 + C_x) - \phi_{i+1,j}^n (1 - C_x)] + \frac{C_y}{2}[\phi_{i,j-1}^n (1 + C_y) - \phi_{i,j+1}^n (1 - C_y)], \tag{25}$$

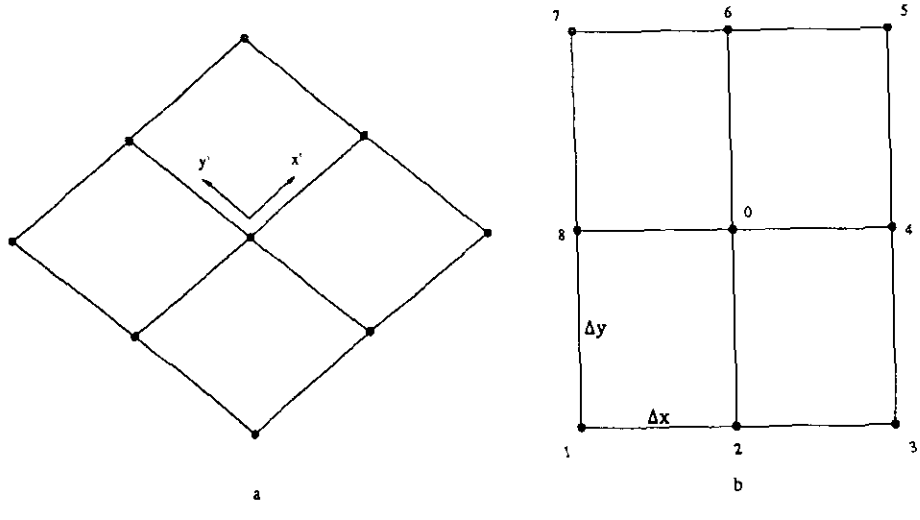

FIG. 2. Computational molecules on (a) general quadrilateral grid, (b) regular rectangular grid.

where $C_x = u_x \Delta t/\Delta x$ and $C_y = u_y \Delta t/\Delta y$ are the *residual* Courant numbers based on the *residual* velocity $\mathbf{u}_R = u_x \hat{\mathbf{i}} + u_y \hat{\mathbf{j}}$. The stability of (25) is examined by studying solutions of the form

$$\phi_{(x,y,t)} = e^{I(k_x x + k_y y + \omega t)}, \tag{26}$$

where k_x and k_y are the wave numbers and $I = \sqrt{-1}$. Substituting (26) into (25) and dividing through by ϕ^n_{ij} yields

$$\begin{aligned} e^{I(\theta_x p + \theta_y q + \omega \Delta t)} = 1 &- C_x^2(1 - \cos\theta_x) - C_y^2(1 - \cos\theta_y) \\ &- C_x C_y \sin\theta_x \sin\theta_y \\ &- I(C_x \sin\theta_x + C_y \sin\theta_y), \end{aligned} \tag{27}$$

where $\theta_x = k_x \Delta x$ and $\theta_y = k_y \Delta y$. By definition $\max(|C_x|, |C_y|) \leqslant 0.5$. Therefore, the sum of the squares of the real and the imaginary parts on the right-hand side of (27) does not exceed unity, thus assuring the realty of ω, i.e., the unconditional stability of (25).

The damping of the scheme is examined by assuming the solution to (25),

$$\phi^n_{i,j} = A^n e^{I(i\theta_x + j\theta_y)}, \tag{28}$$

where $A = A_{(C_x, C_y, \theta_x, \theta_y)}$ is the (complex) damping coefficient which is equal to the right-hand side of (27). Clearly, stability of the scheme implies that $|A|^2 \leqslant 1$. Since the damping depends upon four independent variables it is not amenable to examination by, for example, plotting the damping factor as a function of some of the independent variables while holding the others at constant values. However, some insight into the damping of the scheme may be gained by averaging $|A|^2$ over all possible values of the four independent variables using the equation

$$\begin{aligned} \overline{|A|^2} = \frac{1}{4\pi^2} \int_0^{2\pi} d\theta_y \int_0^{2\pi} d\theta_x \int_{-1/2}^{1/2} dC_y \\ \times \int_{-1/2}^{1/2} dC_x \, |A|^2_{(C_x, C_y, \theta_x, \theta_y)} \end{aligned} \tag{29}$$

which yields the result $\overline{|A|^2} = \frac{5}{6}$. Further insight may be gained by examining the damping of the one-dimensional version of (25) which yields the expression

$$|A|^2 = 1 - C_x^2(1 - C_x^2)(1 - \cos\theta_x)^2, \tag{30}$$

clearly indicating that the damping of the scheme increases with the absolute value of the residual Courant number and that it is independent of the number of grid lengths traveled by the fluid particle during the time step. Since in a non-interpolating semi-Lagrangian Lax–Wendroff scheme the

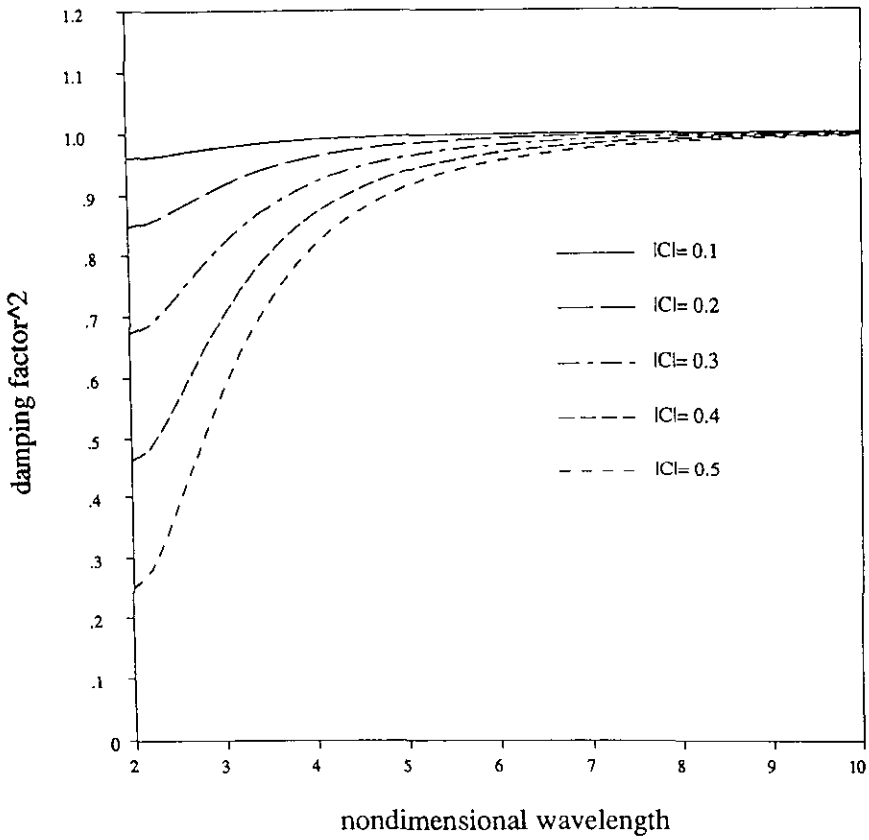

FIG. 3. The square of the magnitude of the damping coefficient, A, as a function of nondimensional wave length for several values of the residual Courant number.

absolute value of the residual Courant number does not exceed 0.5 the damping of this scheme is less than that of an Eulerian Lax–Wendroff scheme in which the value of the Courant number may be as high as 1.0. The value of $|A|^2$ as a function of the residual Courant number C_x and the nondimensional wave lenght $2\pi/k_x \Delta x$ is shown in Fig. 3. The normalised phase speed is also obtained from the one-dimensional version of (25) yielding

$$\frac{u^*}{U} = \frac{1}{p + C_x}\left\{p - \frac{1}{\theta_x}\arctan\left[\frac{-C_x \sin\theta_x}{1 - C_x^2(1-\cos\theta_x)}\right]\right\}, \quad (31)$$

where u^* and U are, respectively, the numerical and the analytical signal propagation speeds. Ideally the normalised phase speed would equal unity. It is clear from (31) that the normalised phase speed asymptotically approaches unity for all wave numbers as the value of p increases. The phase speed as a function of the nondimensional wave length and the residual Courant number is depicted in Figs. 4a to 4d which show the phase speed for $p = 0$, $p = 1$, $p = 2$, and $p = 3$, respectively, and in Figs. 5a and 5b which show the normalised phase speed as a function of the nondimensional wave length and the number of grid lengths traveled by the

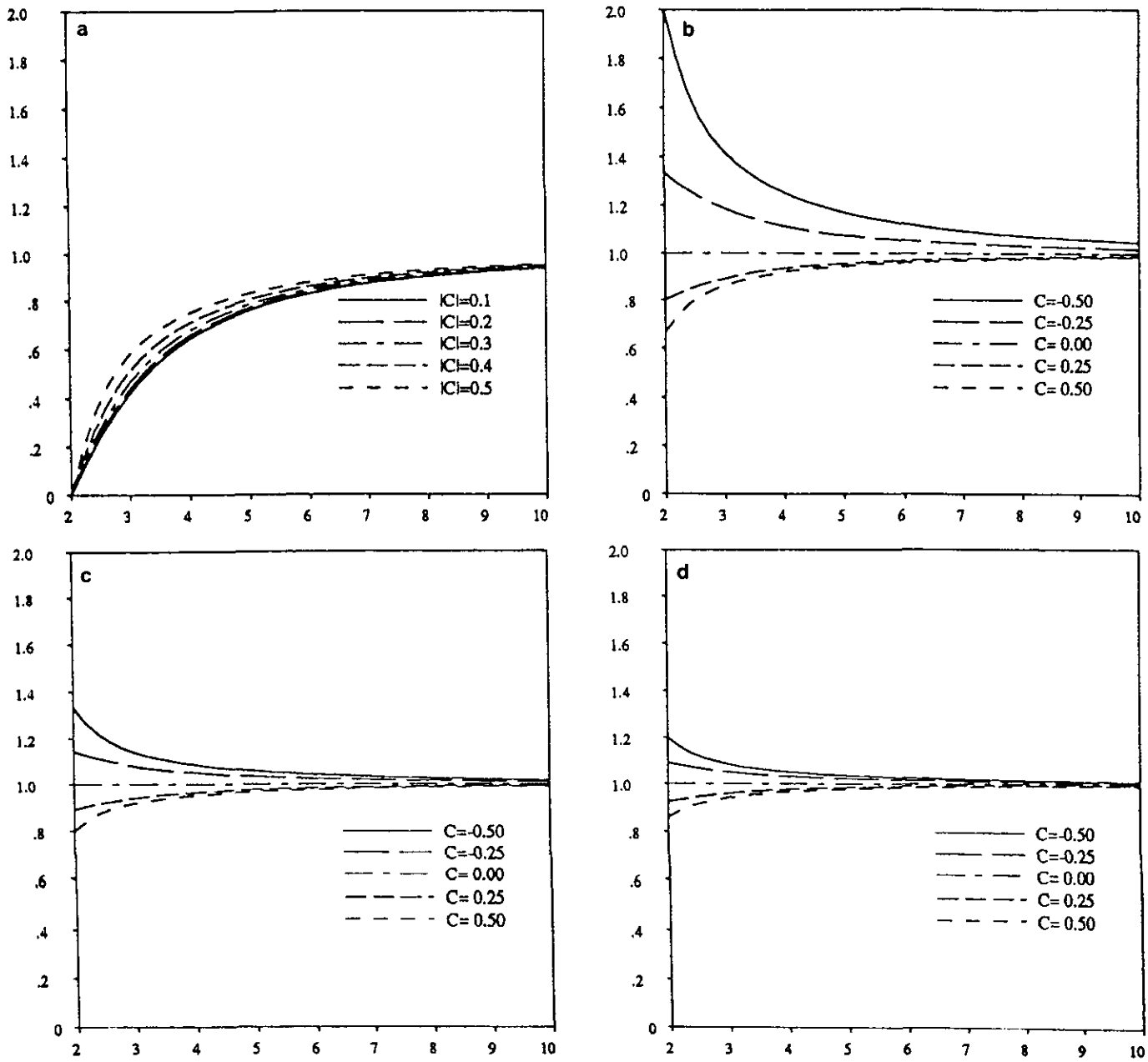

FIG. 4. The normalised phase speed as a function of nondimensional wave length and residual Courant number: (a) $p = 0$; (b) $p = 1$; (c) $p = 2$; (d) $p = 3$.

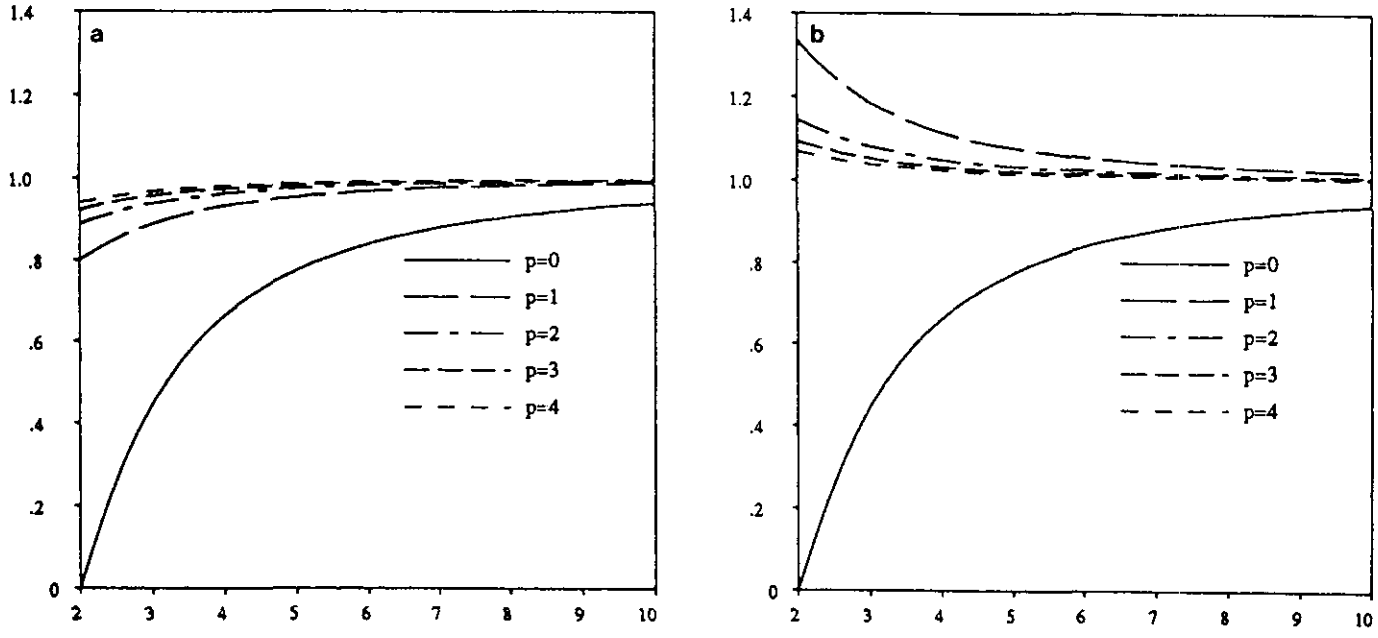

FIG. 5. The normalised phase speed as a function of nondimensional wave length and the number of grid lengths traveled by the fluid particle during the time step: (a) $C_x = 0.25$; (b) $C_x = -0.25$.

fluid particle during the time step for $C_x = 0.25$ and $C_x = -0.25$, respectively. From this discussion of damping and phase speed it is concluded that, although the main purpose of the semi-Lagrangian schemes is to increase the time step of the integration, the suggested Lax–Wendroff scheme offers the serendipitous advantages of weaker damping and improved phase speed when compared to its Eulerian counterpart.

The Lax–Wendroff method which employs the multidimensional Taylor expansion to calculate the spatial derivatives required in (15) is suitable for application on a grid which allows for an inambiguous approximation of these spatial derivatives, such as a grid on which each grid point is connected to five other grid points. However, on an unstructed grid a grid point may be connected to any number of other grid points while employment of the truncated Taylor expansion to calculate the spatial derivatives makes use of the data at five of the surrounding grid points, thus ignoring some of the available information and providing less than optimal accuracy. Another option to calculate the spatial derivatives is by fitting a function of the appropriate differentiability (e.g., $\phi = a_0 + a_1 x + a_2 y + a_3 x^2 + a_4 y^2 + a_5 xy$) to the data in the vicinity of the central point. This simplistic solution, however, offers an extremely limited interpretation of the solution of (11), since it ignores the integral constraint of the conservation of "mass," $\int_\Omega \phi \, d\Omega = \text{const}$. It is therefore suggested that employment of the flux (or control volume) formulation should yield more accurate results than those obtained using the Taylor expansion. The flux formulation is the subject of the next section.

4.2. *The Lax–Wendroff Method Using the Flux Formulation*

The conservation equation (11) is a particular case of the equation

$$\frac{\partial \phi}{\partial t} + \nabla \cdot \mathbf{F} = 0 \tag{32}$$

which is obtained by applying the divergence theorem to the integral conservation law expressed by

$$\frac{\partial}{\partial t} \int_V \phi \, dV + \int_S \mathbf{F} \cdot d\mathbf{S} = 0, \tag{33}$$

where S is the surface enclosing the volume V, and $\mathbf{F} = \phi \mathbf{u}$ is the flux of ϕ. Assuming that ϕ represents the average over V, Eq. (33) may be discretised in time yielding

$$\phi^{n+1} = \phi^n - \frac{\Delta t}{V} \int_S \mathbf{F}^{n+1/2} \cdot d\mathbf{S}, \tag{34}$$

where, to obtain a second-order accuracy in time, the flux integral must be evaluated at the time level $n + \frac{1}{2}$. Assuming a constant advecting velocity, Eq. (34) may be rewritten as

$$\phi^{n+1} = \phi^n - \frac{\Delta t}{V} \mathbf{u} \cdot \int_S \phi^{n+1/2} \, d\mathbf{S}. \tag{35}$$

For numerical solution of (35) the locations of ϕ at times t^n, $t^{n+1/2}$, and t^{n+1} must be defined. Since the values of ϕ^n and

ϕ^{n+1} represent the averages over the volume V these values must be evaluated at the centroid of the volume V, while the value of $\phi^{n+1/2}$ must be known on the surface S. In the computational domain the surface S will normally consist of straight line segments or planes (in two or three dimensions, respectively). Therefore the values of $\phi^{n+1/2}$ need only be known at points where these straight line segments (planes) meet, and the integration over the surface may be performed assuming a linear distribution between these points.

To illustrate this idea let a two-dimensional domain be discretised using a regular rectangular grid generating the computational molecule shown in Fig. 2b. Let the value of ϕ at the grid points be known at some time level n. Clearly, the value of ϕ at the center point of this molecule (point 0) represents the value of ϕ averaged over a rectangle the corners of which are located at the centers of the four rectangles surrounding point 0. The center points of the rectangles may be regarded as grid points of a staggered grid. Once the values of $\phi^{n+1/2}$ at the staggered grid points are known the value of ϕ^{n+1} at point 0 may be calculated using (35). In this calculation the closed line which consists of four straight line segments connecting the staggered grid points serves as the surface S, and the area enclosed by it serves as the volume V. Following a derivation similar to that of Eq. (35) the values of $\phi^{n+1/2}$ at the staggered grid points are calculated using

$$\phi_c^{n+1/2} = \phi_c^n - \frac{\Delta t}{2V}\mathbf{u}\cdot\int_S \phi^n \, d\mathbf{S}, \tag{36}$$

where the subscript c indicates the center of a rectangle, the corners of which are located at the grid points of the primary grid; ϕ_c^n is calculated by averaging the four corner values of ϕ^n, the close line connecting the rectangle corners serves as the surface S, and the area enclosed by it serves as the volume V.

Using the values of ϕ^n at the four corner points of a rectangle whose size is $\Delta x \times \Delta y$ and, assuming linear distribution of ϕ along the lines between the corner points, the integral on the right-hand side of (36) may be evaluated yielding

$$\int_S \phi \, d\mathbf{S} = \hat{\mathbf{i}}\frac{\Delta y}{2}(\phi_{tr} - \phi_{tl} + \phi_{br} - \phi_{bl}) +$$

$$+\hat{\mathbf{j}}\frac{\Delta x}{2}(\phi_{tr} - \phi_{br} + \phi_{tl} - \phi_{bl}), \tag{37}$$

where the subscripts t, b, r, and l indicate, respectively, top, bottom, right, and left, with respect to the center of the rectangle. For example, ϕ_{tr} is the value of ϕ at the top right corner. Substitution of (37) into (36) yields the values of $\phi_c^{n+1/2}$ at the centers of the four rectangles surrounding the center point of the computational molecule. These values may now be used as corner points in (37) to evaluate the integral on the right-hand side of (35), and, after some simple algebra, the expression obtained is

$$\phi^{n+1} = \phi^n - \Delta t(u\overline{\phi_x} + v\overline{\phi_y}) + \frac{\Delta t^2}{2}(u^2\overline{\phi_{xx}} + 2uv\overline{\phi_{xy}} + v^2\overline{\phi_{yy}}), \tag{38}$$

where

$$\begin{aligned}
\overline{\phi_x} &= \frac{\delta_x\phi_{i,j-1} + 2\delta_x\phi_{i,j} + \delta_x\phi_{i,j+1}}{4} \\
\overline{\phi_{xx}} &= \frac{\delta_{xx}\phi_{i,j-1} + 2\delta_{xx}\phi_{i,j} + \delta_{xx}\phi_{i,j+1}}{4}, \\
\overline{\phi_y} &= \frac{\delta_y\phi_{i-1,j} + 2\delta_y\phi_{i,j} + \delta_x\phi_{i+1,j}}{4}, \\
\overline{\phi_{yy}} &= \frac{\delta_{yy}\phi_{i-1,j} + 2\delta_{yy}\phi_{i,j} + \delta_{yy}\phi_{i+1,j}}{4}, \\
\overline{\phi_{xy}} &= \frac{\phi_{i-1,j-1} + \phi_{i+1,j+1} - \phi_{i+1,j-1} - \phi_{i-1,j+1}}{4\Delta x\,\Delta y},
\end{aligned} \tag{39}$$

and the δ operators are defined by

$$\begin{aligned}
\delta_x T_{k,l} &= \frac{T_{k+1,l} - T_{k-1,l}}{2\Delta x}, \\
\delta_{xx} T_{k,l} &= \frac{T_{k+1,l} - 2T_{k,l} + T_{k-1,l}}{\Delta x^2}, \\
\delta_y T_{k,l} &= \frac{T_{k,l+1} - T_{k,l-1}}{2\Delta y}, \\
\delta_{yy} T_{k,l} &= \frac{T_{k,l+1} - 2T_{k,l} + T_{k,l-1}}{\Delta y^2}.
\end{aligned} \tag{40}$$

Equation (38) conforms to the format of (15) while employing, as may be seen from (39) and (40), weighted averages of second-order approximations to the spatial derivatives. This analysis is also valid if the conservation law expressed by the Eulerian equation (32) is replaced by the noninterpolating semi-Lagrangian formulation,

$$\frac{d\phi}{dt} + \nabla\cdot\mathbf{F}_R = 0, \tag{41}$$

where $\mathbf{F}_R = \phi\mathbf{u}_R$ is the *residual* flux of ϕ. Using the semi-Lagrangian formulation, introduction of (39) into (38) yields

$$\phi_{i+p,j+q}^{n+1} = \phi_{i,j}^{n}\left(1-\frac{C_x^2+C_y^2}{2}\right)+\frac{C_xC_y}{4}$$
$$\times(\phi_{i-1,j-1}^{n}+\phi_{i+1,j+1}^{n}-\phi_{i+1,j-1}^{n}-\phi_{i-1,j+1}^{n})$$
$$+\frac{C_x}{8}[(\phi_{i-1,j-1}^{n}+2\phi_{i-1,j}^{n}+\phi_{i-1,j+1}^{n})(1+C_x)$$
$$-(\phi_{i+1,j-1}^{n}+2\phi_{i+1,j}^{n}+\phi_{i+1,j+1}^{n})(1-C_x)$$
$$-2C_x(\phi_{i,j-1}^{n}+\phi_{i,j+1})]$$
$$+\frac{C_y}{8}[(\phi_{i-1,j-1}^{n}+2\phi_{i,j-1}^{n}+\phi_{i+1,j-1}^{n})(1+C_y)$$
$$-(\phi_{i-1,j+1}^{n}+2\phi_{i,j+1}^{n}+\phi_{i+1,j+1}^{n})(1-C_y)$$
$$-2C_y(\phi_{i-1,j}^{n}+\phi_{i+1,j})]. \tag{42}$$

The stability of this scheme is analyzed by substituting (26) into (42) and dividing through by $\phi_{i,j}^{n}$ which yields

$$e^{I(\theta_x p+\theta_y q+\omega\Delta t)} = 1-\frac{C_x^2}{2}(1-\cos\theta_x)(1+\cos\theta_y)$$
$$-\frac{C_y^2}{2}(1-\cos\theta_y)(1+\cos\theta_x)$$
$$-C_xC_y\sin\theta_x\sin\theta_y$$
$$-I\frac{1}{2}[C_x\sin\theta_x(1+\cos\theta_y)$$
$$+C_y\sin\theta_y(1+\cos\theta_x)]. \tag{43}$$

Since $\max(|C_x|, |C_y|)\leqslant 0.5$ the sum of the squares of the real and the imaginary parts of the right-hand side of (43) does not exceed unity, thus assuring the reality of ω, i.e., the unconditional stability of (42). The damping of the scheme is examined by introducing (28) into (42), and the damping coefficient $A = A_{(C_x,C_y,\theta_x,\theta_y)}$ is equal to the right-hand side of (43). Application of (29) to calculate the average value of $|A|^2$ for this scheme yields the result $\overline{|A|^2} = \frac{11}{12}$ which is closer to unity than the value obtained for the previous scheme, $\overline{|A|^2} = \frac{5}{6}$, thus indicating that the performance of this

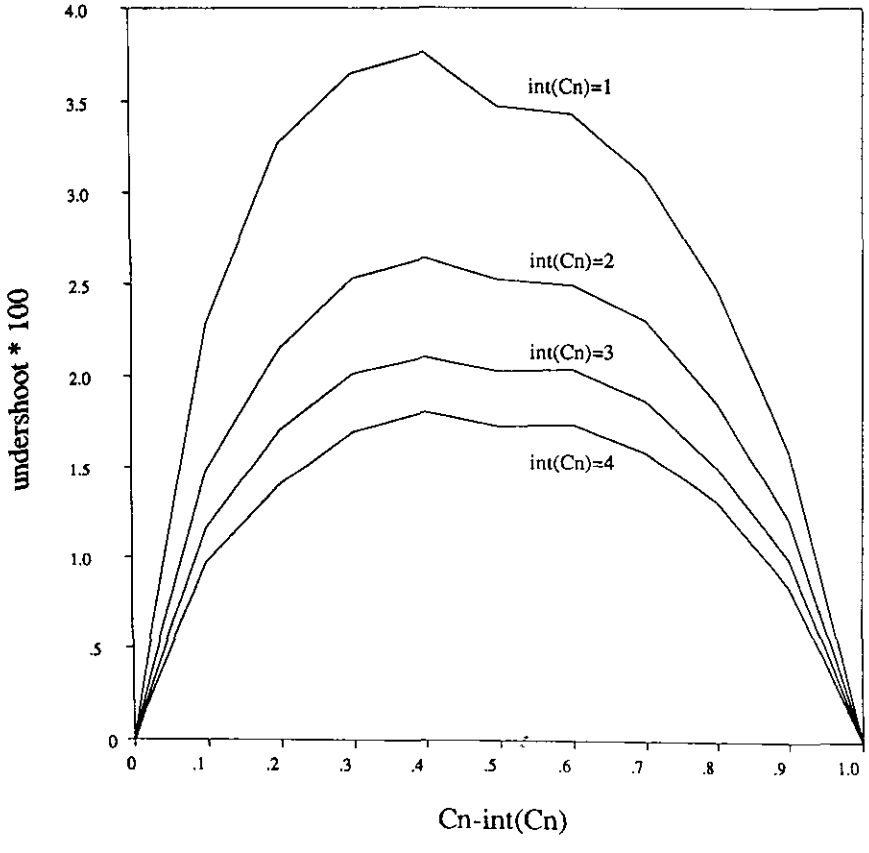

FIG. 6. The L_1 norm of the difference between the analytical and the numerical solutions versus $C-\text{int}(C)$, where $\text{int}(C)$ is the integer part of the Courant number. The results were obtained after five crossings of the 64 x 64 domain by a cosine hill with wave length of 40 grid lengths. The Courant number range is $1.0\leqslant C\leqslant 5.0$.

scheme, which is based on the flux formulation, is superior to the performance of the previous scheme, which is based on the multidimensional Taylor expansion. The expressions for the one-dimensional damping coefficient and the phase speed obtained for this scheme are identical to those obtained for the previous scheme and given by (30) and (31).

It must be noted that the validity of the semi-Lagrangian flux-based scheme given by (42) is by no means limited to a two-dimensional regular rectangular grid, and extensions to three dimensions and unstructured grids are straight forward. It is, however, possible that on some grids the formulation will be only *conditionally* stable thus limiting its utility on such grids to the Eulerian formulation of the advection equation.

5. COMPUTATIONAL EXAMPLES

To demonstrate the viability of the suggested noninterpolating semi-Lagrangian Lax–Wendroff scheme a series of two-dimensional advection tests was performed. The tests consist of advection of different functions by a constant velocity vector. The flux-based scheme given by (42) was employed. In all tests the Courant numbers in the x and y directions were equal. By advecting a fluid particle from the nearest grid point rather than from the true departure point the noninterpolating schemes introduce an error. Clearly, this error grows with the distance between the departure point and the nearest grid point. This error is therefore at its maximum when the residual Courant number is 0.5. To examine the suggested scheme under the least favorable conditions the Courant numbers in both the x and y directions were set at 2.5.

In the first test a cone was generated in a square domain represented on a 64×64 cell Cartesian grid. The radius of the cone at the base was 30 grid lengths. Using periodic boundary conditions the advection was continued until the advected funcion crossed (i.e., exited and re-entered) the

TABLE I

Results of the Tests in Which a Function Is Advected Five Times Across a 64×64 Domain Using the Noninterpolating Semi-Lagrangian Lax–Wendroff Scheme with a Courant Number of 2.5.

Case	Max	Min × 10	Mass	Energy	$L_\infty \times 10$	$L_1 \times 10^2$	$L_2 \times 10^4$
1	0.935	−0.206	1.000	0.999	0.718	0.654	1.53
2	0.986	−0.003	1.000	0.996	0.610	0.433	1.70
3	1.000	−0.117	1.000	1.000	0.122	0.423	0.83
4	0.999	−0.165	1.000	0.999	0.200	0.516	1.14
5	0.996	−0.250	1.000	0.997	0.396	0.620	1.66
6	0.996	−0.419	1.000	0.991	0.896	0.768	2.68
7	0.955	−0.819	1.000	0.960	2.40	0.997	5.03

Note. In case 1 the advected function is a cone with a base radius of 30 grid lengths, in Case 2 it is a Gaussian with half-width of 15 grid lengths, and in Cases 3, 4, 5, 6, and 7 the advected functions are cosine hills with wavelengths of 60, 50, 40, 30, and 20 grid lengths, respectively. The extremal values of the advected function ϕ are listed under *max* and *min*, and the ratios of $\int_\Omega \phi$ and $\int_\Omega \phi^2$ to their initial values are listed as mass and energy, respectively. L_∞, L_1, and L_2 represent the corresponding norms of the difference between the numerical and analytical solutions.

TABLE II

Results of the Test in Which a Cosine Hill with Wavelength of 40 Grid Lengths Is Advected across a 64×64 Domain Using the Noninterpolating-Semi-Lagrangian Lax–Wendroff Scheme with a Courant number of 2.5.

Cross. no.	Max	Min × 10	Mass	Energy	$L_\infty \times 10$	$L_1 \times 10^2$	$L_2 \times 10^4$
0	1.000	0.000	1.000	1.000	0.000	0.000	0.000
1	1.000	−0.088	1.000	0.999	0.088	0.135	0.389
2	0.997	−0.138	1.000	0.999	0.150	0.259	0.718
3	0.997	−0.179	1.000	0.998	0.232	0.384	1.04
4	0.998	−0.216	1.000	0.998	0.311	0.501	1.35
5	0.996	−0.250	1.000	0.997	0.396	0.620	1.66

Note. The cross. column indicates the number of times the function has been advected across the domain (0 indicates initial conditions). The rest of the notation is as in Table I.

TABLE III

Results of the Test in Which a Cosine Hill with Wavelength of 40 Grid Lengths Is Advected across a 64×64 Domain Using the Noninterpolating Semi-Lagrangian Lax–Wendroff Scheme

C	Max	Min × 10	Mass	Energy	$L_\infty \times 10$	$L_1 \times 10^2$	$L_2 \times 10^4$
1.0	1.000	−0.000	1.000	1.000	0.000	0.000	0.00
1.2	0.996	−0.327	1.000	0.998	0.480	0.743	1.97
1.4	0.995	−0.376	1.000	0.996	0.663	1.010	2.67
1.6	0.994	−0.343	1.000	0.996	0.583	0.890	2.36
1.8	0.999	−0.247	1.000	0.999	0.320	0.509	1.36
2.0	1.000	−0.000	1.000	1.000	0.000	0.000	0.00
2.2	1.000	−0.215	1.000	0.999	0.342	0.419	1.13
2.4	0.998	−0.264	1.000	0.998	0.388	0.610	1.63
2.6	0.998	−0.249	1.000	0.998	0.358	0.567	1.52
2.8	0.998	−0.185	1.000	0.999	0.202	0.333	0.909
3.0	1.000	−0.000	1.000	1.000	0.000	0.000	0.000
3.2	0.999	−0.170	1.000	0.999	0.175	0.294	0.807
3.4	0.997	−0.210	1.000	0.998	0.272	0.440	1.19
3.6	0.997	−0.203	1.000	0.998	0.256	0.417	1.13
3.8	0.998	−0.150	1.000	1.000	0.150	0.249	0.689
4.0	1.000	−0.000	1.000	1.000	0.000	0.000	0.000
4.2	1.000	−0.140	1.000	1.000	0.140	0.227	0.630
4.4	0.999	−0.180	1.000	0.999	0.208	0.346	0.948
4.6	0.999	−0.173	1.000	0.999	0.199	0.333	0.912
4.8	0.999	−0.131	1.000	1.000	0.131	0.201	0.562
5.0	1.000	−0.000	1.000	1.000	0.000	0.000	0.000

Note. Data in the table were obtained after five crossings of the domain. The C column indicates the Courant number. The rest of the notation is as in Table I.

domain five times. After each crossing the peak value and the largest undershoot of the advected function, ϕ, were registered, and the ratios of the "mass," $\int_\Omega \phi$, and the "energy," $\int_\Omega \phi^2$, to their initial values were calculated. Also calculated were the L_∞, L_1, and L_2 norms of the error vector, i.e., the difference between the analytical and the numerical solutions at each grid point. After five crossings (which required 128 time steps) the amplitude of the cone at its apex was reduced by 6.5%; the largest undershoot was 2% of the initial peak value, the mass was practically unchanged, and the energy was reduced by 0.1%. The L_∞, L_1, and L_2 norms of the error vector were, respectively, 0.072, 0.654×10^{-2}, and 0.153×10^{-3}. In a second test the advected function was a Gaussian with a half-width of 15 grid lengths. After five crossings its peak value was reduced by 1.4%, the largest undershoot was 0.03% of the initial peak value, the mass was unchanged, and the energy was reduced by 0.4%. The L_∞, L_1, and L_2 norms of the error vector were, respectively, 0.061, 0.433×10^{-2}, and 0.170×10^{-3}. To gain further insight into the performance

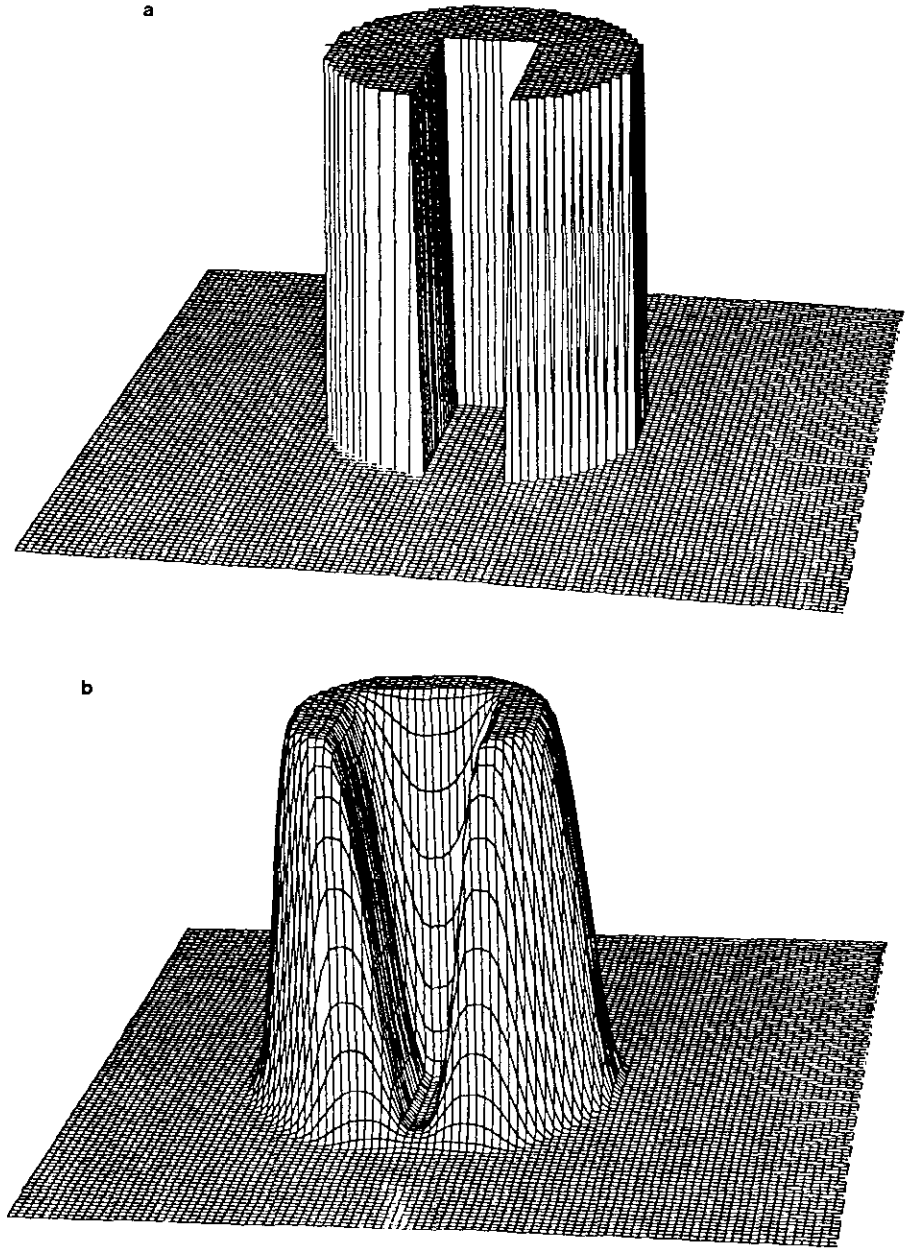

FIG. 7. Advection of a slotted cylinder by FCT-corrected Eulerian and semi-Lagrangian Lax–Wendroff schemes. The initial distribution is depicted in (a), the distributions after four crossings of the domain using an Eulerian scheme with Courant number of 0.5 and a semi-Lagrangian scheme with Courant number of 2.5 are depicted in (b) and (c), respectively.

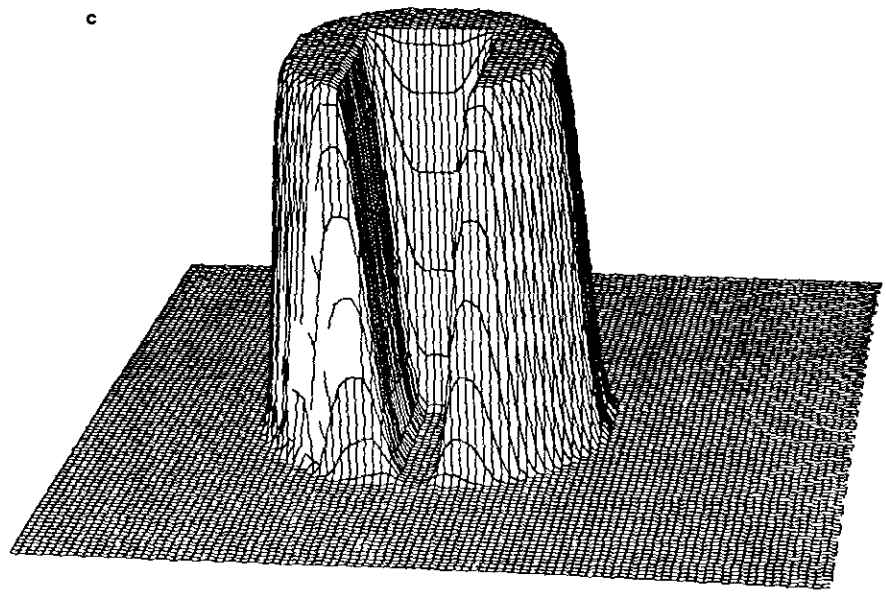

Fig. 7.—Continued

of the method the Gaussian was replaced by a cosine hill whose wave length was 60 grid lengths. After five crossings the peak value, the mass, and the energy were practically unchanged, and the largest undershoot was 1.2% of the initial peak value. The L_∞, L_1, and L_2 norms of the error vector were, respectively, 0.0012, 0.423×10^{-2}, and 0.83×10^{-4}. The same test was performed for cosine hills with wavelengths of 50, 40, 30, and 20 grid lengths. The results of these tests are summarized in Table I and indicate that the algorithm performs very well, with an expected improvement at longer wavelengths. The rate at which the peak and undershoot, the mass and energy ratios, and the three error norms change may be seen from the data given in Table II which lists the values recorded after each crossing for the cosine hill with a wave length of 40 grid lengths. The same test was repeated with different values of the Courant number for the cosine hill with a wave length of 40 grid lengths. Table III lists the data recorded after five crossings of the domain for Courant numbers ranging from 1.0 to 5.0. As can be seen from the data summarized in Tables I, II, and III, the scheme conserves mass extremely well. The mass ratio exhibited variations in the seventh (!) significant digit. As predicted by the phase speed analysis in (31) the results improve as the value of nint(C) increases. This is clearly demonstrated by the values of the L_1 norm of the error vector shown in Fig. 6. It may be seen from this figure that the L_1 error norm improves (i.e., decreases) as int(C) increases for a given $C - \text{int}(C)$, where int(C) is the integer part of the Courant number. For example, the L_1 error norm obtained for $C = 4.4$ is better than that obtained for $C = 3.4$. Also, the results improve as nint(C) increases. For example, the L_1 error norm obtained for $C = 2.8$ is better than that obtained for $C = 2.2$. The results shown in this figure indicate that for $\text{int}(C) = 1$ the worst results are obtained when the noninteger part of the Courant number is somewhat less than 0.5. This is a result of the fact that the quality of the results are adversely affected by an increase in the number of time steps required to complete any given calculation. Thus, although for a single time step $C - \text{int}(C) = 0.5$ constitutes the least favorable condition, when the numer of time steps required to complete a calculation with, say, $C = 1.4$ is sufficiently larger than that required to complete a calculation with $C = 1.5$, the adverse effect of the increased number of time steps is noticeable.

These results, and especially the undershoots, may be significantly improved by employing a monotonicity preserving scheme. Since overshoots and undershoots are generated mainly in the vicinity of steep gradients the advection of a slotted cylinder provides a stringent test of the ability of an advection scheme to preserve monotonicity. The slotted cylinder test was employed in [15] to demonstrate the viability of the FCT correction in a multidimensional domain. Here this test is employed to demonstrate the advantages of the FCT-corrected semi-Lagrangian Lax–Wendroff scheme over its Eulerian counterpart in two dimensions. The square domain was represented on a 100×100 Cartesian grid, and the slotted cylinder was placed in the center of the domain as shown in Fig. 7a. The diameter of the cylinder was 40 grid lengths, the width of the "bridge" connecting the two cylinder halves was 15 grid lengths, and the width of the gap was 12 grid lengths. An Eulerian FCT-correctd Lax–Wendroff scheme was employed to advect this cylinder through the domain four times. The Courant number in this test was 0.5 in both directions; i.e., 800 time steps were required to complete the test. The result is depicted in Fig. 7b. The advection test was

repeated with a FCT-corrected semi-Lagrangian Lax–Wendroff method using a Courant number of 2.5, thus requiring 80 time steps (as explained earlier, a residual Courant number of 0.5 is the least favorable for the scheme). The result of this test is depicted in Fig. 7c. The results of the two tests are compared by examining the filling-in of the gap, erosion of the bridge, and the sharpness of the profile defining the surface of the cylinder. The performance of the semi-Lagrangian scheme is clearly superior to that of its Eulerian counterpart.

6. CONCLUSIONS

A truly noninterpolating semi-Lagrangian method has been develped. It is based upon a modification of the one-step Lax–Wendroff algorithm and is unconditionally stable on a regular rectangular grid. The algorithm is explicit and is second-order accurate in both time and space. It may be converted into a monotonicity-preserving scheme following exactly the same steps required for similar conversion of a traditional Lax–Wendroff algorithm. Being explicit and truly noninterpolating, the suggested algorithm requires the least possible computation cost for an algorithm of this order of accuracy. At the same time it is a two-time level algorithm thus requiring the least possible allocation of computer memory for data storage. Our numerical experiments indicate that the algorithm is extremely accurate.

ACKNOWLEDGMENT

The comments made by W. R. Peltier on an earlier draft of this paper are gratefully acknowledged.

REFERENCES

1. J. P. Benque, B. Ibler, and G. Labadie, *Numerical Methods for Non-Linear Problems, Vol. 1*, edited by C. Taylor (Pineridge Press, Swansea, UK, 1980), p. 709.
2. D. L. Book, J. P. Boris, and K. Hain, *J. Comput. Phys.* **18**, 248 (1975).
3. J. Donea, *J. Numer. Methods Eng.* **20**, 101 (1984).
4. A. Harten, B. Enquist, S. J. Osher, and S. R. Chakravarthy, *J. Comput. Phys.* **71**, 231 (1987).
5. W. N. G. Hitchon, D. J. Koch, and J. B. Adams, *J. Comput. Phys.* **83**, 79 (1989).
6. T. J. R. Hughes, *The Finite Element Method* (Prentice Hall, Englewood Cliffs, NJ, 1987).
7. S. R. Karpik, *Ocean Wave Mechanics, Computational Fluid Dynamics and Mathematical Modelling, Halifax, Canada, 1990*, edited by M. Rahman (Computational Mechanics, Boston, 1990), p. 895.
8. E. S. Oran and J. P. Boris, *Numerical Simulation of Reactive Flow* (Elsevier Science, New York, 1987).
9. P. J. Roache, *Computational fluid dynamics* (Hermosa, Albuquerque, NM, 1976).
10. A. Robert, *Atmos. Ocean.* **19**, 35 (1981).
11. H. Ritchie, *Mon. Weather Rev.* **114**, 135 (1986).
12. G. D. Smith, *Numerical Solutions of Partial Differential Equations: Finite Difference Methods*, 3rd ed. (Clarendon Press, Oxford, 1987).
13. P. K. Smolarkiewicz and P. J. Rasch, *J. Atmos. Sci.* **48** (6), 793 (1991).
14. A. Staniforth and J. Cote, *Mon. Weather Rev.* **119**, 2206 (1991).
15. S. T. Zalesak, *J. Comput. Phys.* **31**, 335 (1979).